# Formaldehyde around 3.5 and 5.7-μm: Measurement and calculation of broadening coefficients

D. Jacquemart [a,b,*], A. Laraia [c], F. Kwabia Tchana [a,b,1], R.R. Gamache [c], A. Perrin [d], N. Lacome [a,b]

[a] UPMC Univ Paris 06, UMR 7075, Laboratoire de Dynamique, Interactions, et Réactivité (LADIR), F-75005, Paris, France
[b] CNRS, UMR 7075, Laboratoire de Dynamique, Interactions, et Réactivité (LADIR), F-75005, Paris, France
[c] University of Mass Lowell, Department of Environmental, Earth & Atmospheric Sciences, Lowell, MA 01854, USA
[d] Laboratoire Interuniversitaire des Systèmes Atmosphériques (LISA), CNRS/Univ Paris Est & Paris 7, 61 avenue du Général de Gaulle, 94010 Créteil cedex, France

## ARTICLE INFO

## ABSTRACT

Self- and $N_2$-broadening coefficients of $H_2CO$ have been retrieved in both the 3.5 and 5.7-μm spectral regions. These coefficients have been measured in FT spectra for transitions with various $J$ (from 0 to 25) and $K$ values (from 0 to 10), showing a clear dependence with both rotational quantum numbers $J$ and $K$. First, an empirical model is presented to reproduce the rotational dependence of the measured self- and $N_2$-broadening coefficients. Then, calculations of $N_2$-broadening of $H_2CO$ were made for some for 3296 $v_2$ transitions using the semi-classical Robert–Bonamy formalism. These calculations have been done for various temperatures in order to obtain the temperature dependence of the line widths. Finally, self- and $N_2$-broadening coefficients, as well as temperature dependence of the $N_2$-widths has been generated to complete the whole HITRAN 2008 version of formaldehyde (available as supplementary materials).

© 2010 Elsevier Ltd. All rights reserved.

## 1. Introduction

Both the 3.5 and 5.7 μm spectral regions of formaldehyde are used for the optical detection of this molecule in the atmosphere [1–11]. The importance of the 3.5 and 5.7 μm regions of formaldehyde ($H_2CO$) has been presented in our previous work [12], in which line intensity measurements and calculation have been performed in both spectral regions. These new calculations [12] have been used to update and complete the HITRAN 2008 edition [13] on formaldehyde. For a more accurate detection of formaldehyde in the atmosphere, the knowledge of accurate air-broadening coefficients is necessary as well as their temperature dependence. Spectra of formaldehyde broadened by $N_2$ have been recorded in Paris (LADIR) using a Bruker HR-120 FT-spectrometer. Both self- and $N_2$-broadening coefficients have been measured for numerous transitions in both spectral regions, allowing the observation of rotational dependences with respect to both $J$ and $K$ rotational quantum numbers. A polynomial expansion has been used to reproduce the measurements and their rotational dependences. Theoretical calculations of $N_2$-broadening of $H_2CO$ were performed for 3296 $v_2$ transitions using the semi-classical Robert–Bonamy formalism. These calculations have been done for various temperatures in order to obtain the temperature dependence of the line widths. The goal of this work is to complete the HITRAN line list of formaldehyde with both self- and $N_2$-broadening coefficients, as well as with the $N_2$-broadening temperature dependence.

The experimental conditions of the spectra recorded in this work are detailed in Section 2. The measurements are presented in Section 3 together with the polynomial expansion used to model them. The theoretical calculation of $N_2$-broadening coefficients is detailed in

---

Section 4 while Section 5 presents a comparison with the measurements obtained in this work and others works. Section 6 treats of the temperature dependence as extracted from the optimized theoretical calculations. Finally, the generation of a complete line list for form-aldehyde at 3.6 and 5.7 μm in HITRAN format [13] is presented in Section 7 and will be made available as supplementary materials.

## 2. Experimental details

All the experimental spectra used in this work have been recorded using the Bruker IFS 120 HR Fourier transform spectrometer of LADIR in Paris. For all spectra, the instrument was equipped with a MCT photovoltaic detector, a Ge/KBr beamsplitter, and a Globar source. The whole optical path was under vacuum, and a 0.8 mm entrance aperture diameter was used. No optical filter has been used in order to measure both the 3.6 and 5.7 μm spectral regions of form-aldehyde absorption with the same spectra. The recorded spectral domain is located between 1400 and 4000 $cm^{-1}$. Each spectrum was the result of the co-addition of 100 interferograms (an over sampling ratio of 8 has been used by post-zero filling the interferograms, but no numerical apodization has been performed). A 30 cm stainless steel cell

**Table 1**
Experimental conditions of the recorded spectra.

| Spectrum No | Pressure of $H_2CO$ (hPa) | Pressure of $N_2$ (hPa) | Temperature (K) |
|---|---|---|---|
| 1 | 0.480 | | 297.7 |
| 2 | 0.536 | | 297.2 |
| 3 | 0.577 | | 297.8 |
| 4 | 0.657 | | 298.3 |
| 5 | 0.491 | 14.76 | 298.6 |
| 6 | 0.556 | 19.76 | 298.7 |
| 7 | 0.587 | 28.65 | 298.3 |
| 8 | 0.658 | 37.94 | 298.6 |

*Absorbing sample*: Natural $H_2CO$ (98.624% of $H_2C^{16}O$); Estimated purity ~98.9 %. *Experimental conditions*: SNR=75–100; Absorption path=30 cm.

closed by two KBr windows has been used. More details on the experimental set-up can be found in Ref. [12]. The experimental conditions of spectra used in this work are summarized in Table 1.

## 3. Measurements

### 3.1. Data reduction

Based on the 4 experimental spectra recorded with pure $H_2CO$ gas (see conditions in Table 1 for spectra 1–4), the multispectrum fitting procedure described in Ref. [14] has been used to retrieve the line positions, intensities, and self-broadening coefficients [12]. The Voigt profile has been used to retrieve line parameters and no significant signatures have been observed in the residuals of the fit. In order to avoid polymerization, low pressures of $H_2CO$ have been used. Consequently, even in the case of quite large self-broadening coefficients (around 0.5 $cm^{-1}$/atm), the determination of these coefficients cannot be very accurate. For spectra 5–8, recorded for a mixture of $H_2CO$–$N_2$, the contribution of the self-broadened widths is not completely negligible. In a first step the self-broadening coefficients have been obtained from spectra 1–4 and modelled using a polynomial expansion that allowed reproducing the rotational dependence with respect in $J$ and $K_a$ of the lower state of the transitions (see Section 3.2). In the following, the notations $J$, $K_a$ and $K_c$ are the quantum numbers associated to the lower state of the transition. When performing the fit of spectra 5–8, the self-broadening coefficients were constrained to the values obtained from the empirical polynomial expansion described later in Section 3.2.

Finally, 284 and 368 self-broadening coefficients have been retrieved respectively, in the 5.7 and 3.6-μm spectral regions, respectively, and 280 and 456, $N_2$-broadening coeffi-cients in the same spectral regions, respectively. All these measurements have been gathered in Table A1 and A2 (see supplementary data), given as supplementary materials and are plotted versus $J$ in Fig. 1 for the self-broadening coeffi-cients, and in Fig. 2 for the $N_2$-broadening ones. These figures show a clear rotational dependence with respect to $J$.



**Fig. 1.** Self-broadening coefficients versus $J$.

The large dispersion of the measurements in these figures partially hides the rotational dependence with respect to $K_a$. Indeed, when measurements for same $J$ values are plotted versus $K_a$, a $K_a$ rotational dependence is revealed for both self- and $N_2$-broadening coefficients. For a set of broadening coefficients with same value of $J$, the widths decrease with increasing $K_a$. Such dependence has already been pointed out for other molecules [15–22]. As an example, this dependence is plotted in Figs. 3 and 4 partially hides for the self- and $N_2$-broadening coefficients, respectively, for the same $J$ value ($J$=8). Let us recall that the spectra have been recorded with low pressures of formaldehyde in order to avoid polymerization. As a consequence, the self-broadening coefficients are not determined as accurately as the $N_2$-broadening coefficients. The accuracy for the self-broadening coefficients is estimated to range between 10 and 20%, whereas for the $N_2$-broadening coefficients it has been estimated to be between 5 and 10%. For both self- and $N_2$-broadening coefficients, no rotational dependence has been observed with

respect to the $K_c$ quantum numbers or with the type of transitions (corresponding to various values of $\Delta J$, $\Delta K_a$, or $\Delta K_c$).

## 3.2. Empirical polynomial expansion

An empirical polynomial expansion has been used to reproduce both the $J$ and $K_a$ rotational dependence for the self- and $N_2$-broadening coefficients measured in this work. Such a model has already been presented previously for $CH_3Br$ [22]. Each set of the same value of $J$ was fit with a quadratic polynomial expansion in $K_a$ (with first order term constrained to zero):

$$\gamma_J(K_a) = a_J^0 + a_J^2 K_a^2 \qquad (1)$$

Example of the rotational dependence versus $K_a$ (for $J$=8) is plotted in Fig. 3 for the self-broadening coefficients and Fig. 4 for the $N_2$-broadening ones. The two parameters $a_J^0$ and $a_J^2$ have then been plotted versus $J$ in Figs. 5 and 6 for the self- and $N_2$-broadening coefficients, respectively.
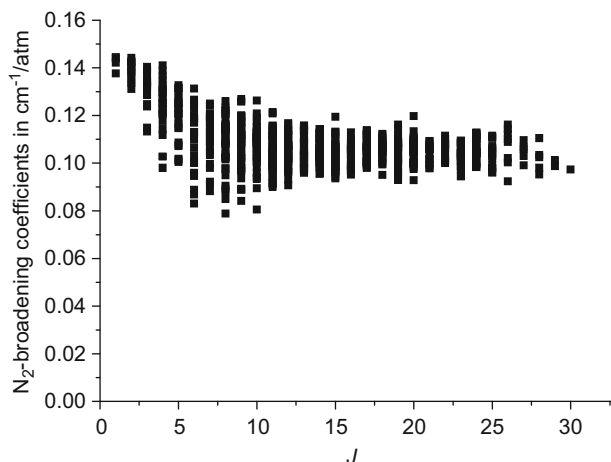


**Fig. 2.** $N_2$-broadening coefficients versus $J$.
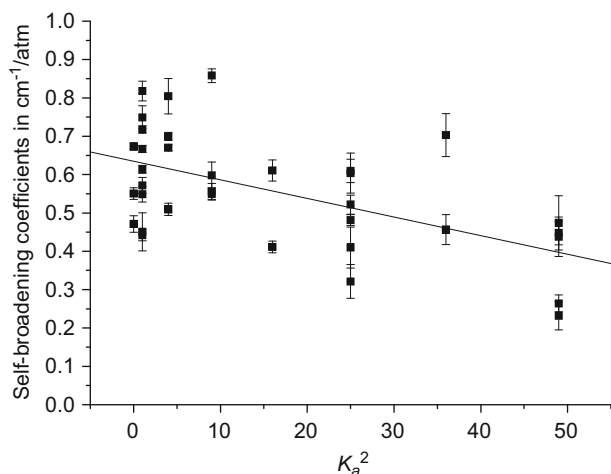


**Fig. 3.** Rotational dependence with respect to $K_a^2$ for self-broadening coefficients with $J$=8. Black squares are the experimental values of this work with 1SD as error bars, whereas the continuous line is the quadratic polynomial expansion fit using Eq. (1).

The continuous line in Figs. 5 and 6 corresponds to a smoothing of the values deduced from experimental measurements. The smoothed values of $a_J^0$ and $a_J^2$ are given in Table 2 and can be used to generate broadening parameters for $J$ and $K_a$ values ranging from 0 to 30 and

0 to 7, respectively. In Figs. 7 and 8 are plotted, for $K_a$ equal to 0 to 7, both experimental broadening coefficients and the calculated ones using Eq. (1) with the parameters of Table 2. Also present in Fig. 8 are the calculated half-widths. Note as $K_a''$ increases the calculations do not agree
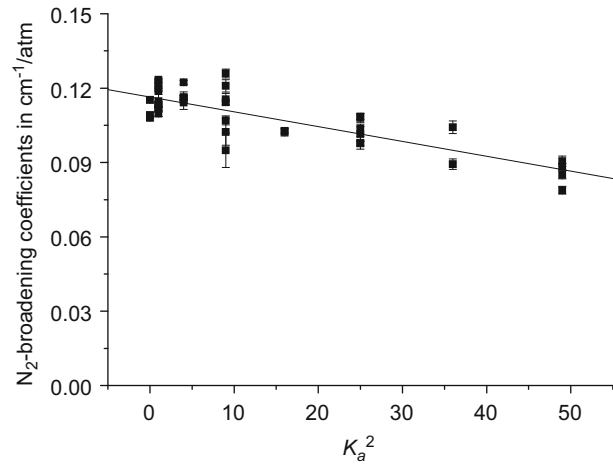


**Fig. 4.** Rotational dependence with respect to $K_a^2$ for N$_2$-broadening coefficients with $J$=8. Black squares are the experimental values of this work with 1SD as error bars, whereas the continuous line is the quadratic polynomial expansion fit using Eq. (1).
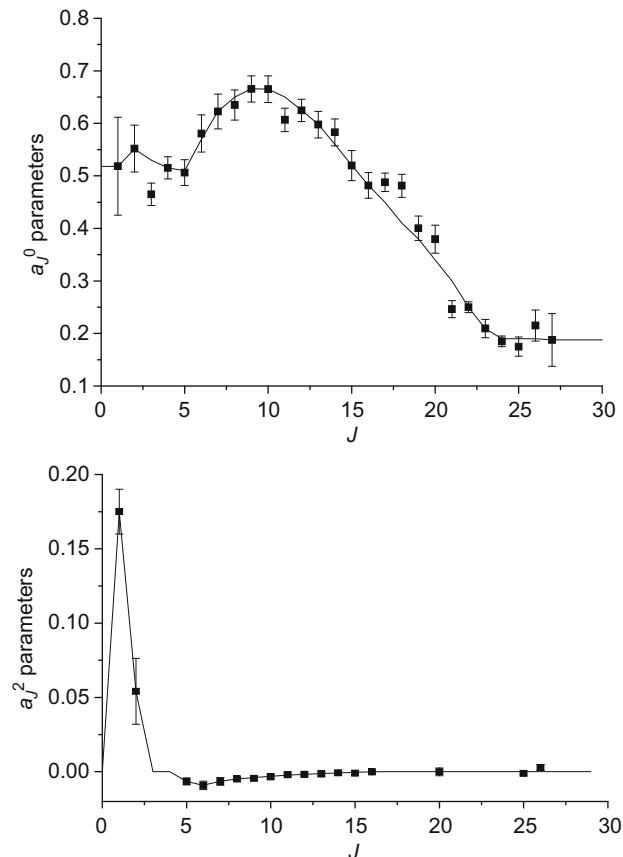


**Fig. 5.** Parameters $a_J^0$ and $a_J^2$ deduced from the fit of the measured self-broadening coefficients using Eq. (1). The error bars are 1SD. The continuous line symbolizes a manual smooth of these parameters.
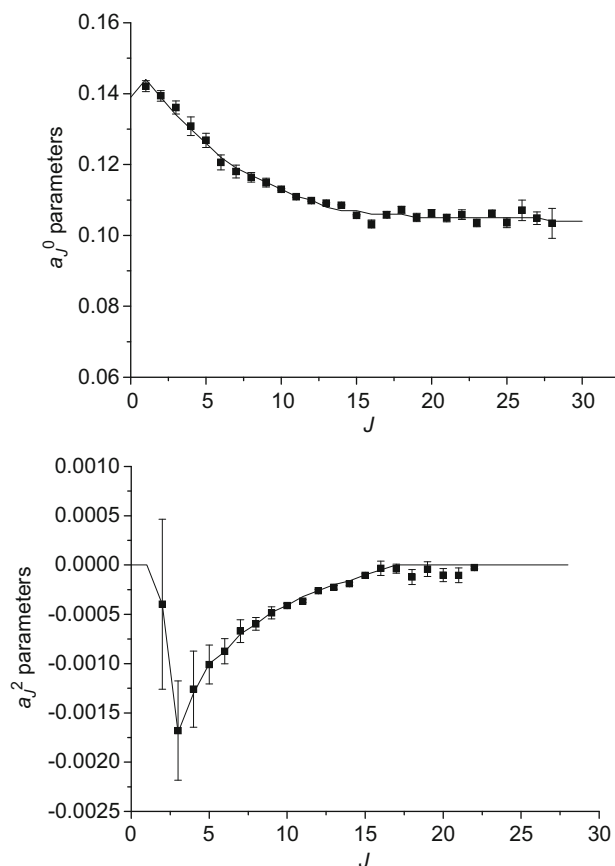
**Fig. 6.** Parameters $a_J^0$ and $a_J^2$ deduced from the fit of the measured $N_2$-broadening coefficients using Eq. (1). The error bars are 1SD. The continuous line symbolizes a manual fit of these parameters.

as well with the measurements. This could be due to the quality of the wavefunctions from diagonalizing the Watson Hamiltonian for high $J$ and $K_a$ states. It is also noted that the adjustment of the intermolecular parameters (see below) in the calculations was done fitting to data with $K_a'' \leq 3$.

The $a_J^0$ parameters represent the $J$ dependence of the broadening parameters for $K_a=0$, whereas the $a_J^2$ parameters describe the influence of the rotational quantum number $K_a$ on broadening parameters. Despite the important dispersion of the measurements, especially for the self-broadening coefficients, the $a_J^0$ and $a_J^2$ parameters reproduced quite well the rotational dependences in Figs. 3, 4, 7 and 8. A part of the scattering of the broadening coefficients in Figs. 1 and 2 is due to the $K_a$ rotational dependence of the widths modelled by the $a_J^2$ parameters.

## 4. Theoretical calculation for $N_2$-broadening coefficients

### 4.1. The complex Robert–Bonamy formalism

The calculations made here are a complex implementation [23–25] of the semi-classical theory of Robert and Bonamy [26]. The complex Robert–Bonamy (CRB) formalism produces the half-width and line shift from a single

complex calculation. In this formalism the half-width, $\gamma$, and line shift, $\delta$, of a ro-vibrational transition $f \leftarrow i$ are given by minus the imaginary part and the real part, respectively, of the diagonal elements of the complex relaxation matrix [27,28]. In computational form $\gamma$ and $\delta$ are expressed in terms of the Liouville scattering matrix:

$$(\gamma - i\delta) = \frac{n_2}{2\pi c} \langle v [1 - e^{-^R S_2(f,i,J_2,v,b)} e^{-i^I S_2(f,i,J_2,v,b)}] \rangle_{v,b,J_2} \tag{2}$$

where $n_2$ is the number density of perturbers and $\langle \ \rangle_{v,b,J_2}$ represents an average over all trajectories (impact parameter $b$ and initial relative velocity $v$) and initial rotational state $J_2$ of the collision partner. $S_2 = {}^R S_2 + i^I S_2$ is the second order terms in the successive expansion of the scattering matrix, which depends on the ro-vibrational states involved and associated collision induced jumps from these levels, on the intermolecular potential and characteristics of the collision dynamics. Note, Eq. (2) generally contains the vibrational dephasing term, $S_1$, which arises only for transitions where there is a change in the vibrational state. The potential leading to $S_1$ is written in terms of the isotropic induction and London dispersion interactions which depend on the vibrational dependence of the dipole moment and polarizability of the radiating molecule. These parameters are not available for $H_2CO$ and the $S_1$ term has been omitted from the

**Table 2**
Parameters $a_J^0$ and $a_J^2$ retained for the calculation of the self- and N$_2$-broadening coefficients using Eq. (1).

| J | Self-broadening coefficients | | N$_2$-broadening coefficients | |
|---|---|---|---|---|
| | $a_J^0$ | $a_J^2$ | $a_J^0$ | $a_J^2$ |
| 0 | 0.518 | 0.0 | 0.1390 | 0.0 |
| 1 | 0.518 | 0.175 | 0.1440 | 0.0 |
| 2 | 0.551 | 0.054 | 0.1388 | −0.00040 |
| 3 | 0.530 | 0.0 | 0.1340 | −0.00170 |
| 4 | 0.515 | 0.0 | 0.1297 | −0.00130 |
| 5 | 0.510 | −0.00654 | 0.1259 | −0.00100 |
| 6 | 0.570 | −0.00921 | 0.1225 | −0.00088 |
| 7 | 0.623 | −0.00648 | 0.1195 | −0.00070 |
| 8 | 0.650 | −0.00485 | 0.1168 | −0.00060 |
| 9 | 0.666 | −0.00400 | 0.1145 | −0.00048 |
| 10 | 0.665 | −0.00300 | 0.1126 | −0.00041 |
| 11 | 0.650 | −0.00230 | 0.1109 | −0.00032 |
| 12 | 0.625 | −0.00178 | 0.1095 | −0.00026 |
| 13 | 0.598 | −0.00120 | 0.1084 | −0.00020 |
| 14 | 0.560 | −0.00075 | 0.1075 | −0.00016 |
| 15 | 0.520 | −0.00040 | 0.1067 | −0.00001 |
| 16 | 0.482 | −0.00013 | 0.1062 | −0.00005 |
| 17 | 0.450 | 0.0 | 0.1058 | 0.0 |
| 18 | 0.410 | 0.0 | 0.1055 | 0.0 |
| 19 | 0.380 | 0.0 | 0.1054 | 0.0 |
| 20 | 0.340 | 0.0 | 0.1053 | 0.0 |
| 21 | 0.300 | 0.0 | 0.1053 | 0.0 |
| 22 | 0.250 | 0.0 | 0.1053 | 0.0 |
| 23 | 0.209 | 0.0 | 0.1053 | 0.0 |
| 24 | 0.190 | 0.0 | 0.1052 | 0.0 |
| 25 | 0.190 | 0.0 | 0.1052 | 0.0 |
| 26 | 0.190 | 0.0 | 0.1050 | 0.0 |
| 27 | 0.188 | 0.0 | 0.1048 | 0.0 |
| 28 | 0.188 | 0.0 | 0.1040 | 0.0 |
| 29 | 0.188 | 0.0 | 0.1040 | 0.0 |
| 30 | 0.188 | 0.0 | 0.1040 | 0.0 |

calculation. Note also, for collision systems with a strong electrostatic component, like H$_2$CO–N$_2$, the effect of the $S_1$ term on the half-width often tends to be small. The exact form of the $S_2$ term is given in Refs. [23–26].

The intermolecular potential used in the calculations is comprised of an electrostatic component (dipole and quadrupole moments of H$_2$CO with the quadrupole moment of N$_2$ or with the dipole and quadrupole moments of H$_2$CO) and an atom–atom component. The initial heteronuclear Lennard–Jones parameters for the atomic pairs are determined using the "combination rules" of Hirschfelder et al. [29]. The atom–atom distance, $r_{ij}$ is expressed in terms of the center of mass separation, $R$, via the expansion in $1/R$ of Sack [30] using the formulation of Neshyba and Gamache [31] expanded to eighth order.

The dynamics of the collision process use Robert and Bonamy's [26] second order in time approximation to the true trajectories, which are based on the isotropic part of the intermolecular potential. These curved trajectories have been shown to accurately model the true trajectories [32].

### 4.2. Parameters for the H$_2$CO–N$_2$ collision system

The wavefunctions used to evaluate the reduced matrix elements are obtained by diagonalizing the Watson Hamiltonian [33] in a symmetric top basis.

The wavefunctions for the ground vibrational state of H$_2$CO are determined using the Watson Hamiltonian constants of Muller et al. [34] and those for the $\nu_2$ vibrational state use the Watson constants of Perrin [35]. The molecular constants for N$_2$ are from Huber and Herzberg [36].

The molecular constants used in the calculations are as follows: The dipole moment is from the work of Fabricant et al. [37], $\mu$=2.33 D. The quadrupole moments are from Kukolich [38] here reported with H$_2$CO in the $I^R$ representation: $Q_{xx}= -0.269 \pm 0.20 \times 10^{-26}$ esu, $Q_{yy}=+0.3295 \pm 0.12 \times 10^{-26}$ esu, $Q_{zz}= -0.0605 \pm 0.16 \times 10^{-26}$ esu. The quadrupole moment of nitrogen is from Mulder et al. [39], $Q_{zz}= -1.4 \pm 0.1 \times 10^{-26}$ esu. The starting atom–atom parameters were obtained using the standard combination rules with the atom–atom parameters for homonuclear diatomics determined by Bouanich [40] by fitting to second virial coefficient data. In the calculations, the atom–atom potential is expanded to eighth order in the molecular centers of mass separation.

The input Lennard–Jones atom–atom parameters are not as well known as the other parameters; the $\varepsilon$ values can vary by 30% and the $\sigma$ values by 5% depending on the source and the $\varepsilon$ values can vary by 69% and the $\sigma$ values by 9% depending on whether they were derived using viscosity data or virial data [29]. Depending on how the values were derived it is possible to find examples in the literature where the parameters for the same interaction pair differ by factors of 2. Thus it appears reasonable to adjust the atom–atom parameters and/or the resulting trajectory parameters provided there are reliable experimental data to fit to. To accomplish this, the measured spectra were studied to identify transitions for which we had high confidence in the measurement. This analysis yielded 39 transitions for the H$_2$CO–N$_2$ system.

For H$_2$CO–N$_2$ there are 6 atom–atom parameters ($\varepsilon_{HN}$, $\sigma_{HN}$, $\varepsilon_{CN}$, $\sigma_{CN}$, $\varepsilon_{ON}$, and $\sigma_{ON}$) that need to be adjusted. Starting from the combination rule values, see Table 3, individually each epsilon or sigma value was increased by 5% and calculations made. These results were compared to the values calculated using the combination rule values yielding a sense of how the half-width varies with the atom–atom parameters. Using these changes as a guide the parameters were varied and calculations made and compared with the 39 measured half-widths (see comparisons between the measured and calculated values in Table 4). After 14 iterations the percent difference went from the initial value of −11.1 to a final value of 0.1. The final atom–atom parameters for the H$_2$CO–N$_2$ system are given in Table 3. Note, the adjustment of the atom–atom parameters was done without the use of a least-squares technique due to the complexity of the atom–atom potential and the time required for a single calculation (∼4 h).

### 4.3. Calculation of half-widths at various temperatures

A file of 3713 transitions in the $\nu_2$, $\nu_3$, and $\nu_5$ bands of H$_2$CO [35] in the frequency range 1620–1840 cm$^{-1}$ atm$^{-1}$
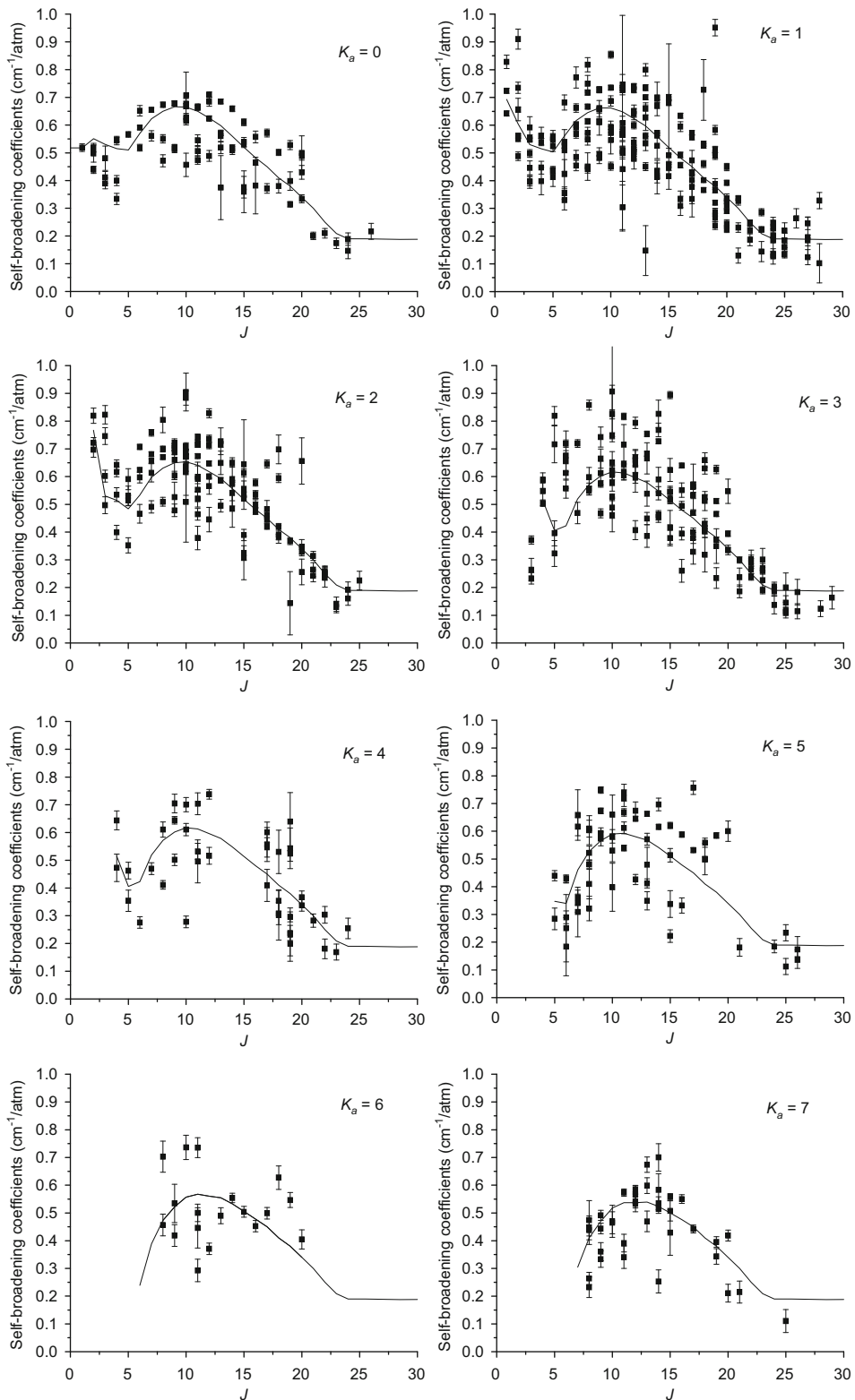
**Fig. 7.** Self-broadening coefficients measurements are plotted (solid squares) for each value of $K_a$ (from 0 up to 7). The error bars are 1SD. The continuous line represents calculation based on an empirical expansion (see Eq. (1)) and parameters of Table 2.
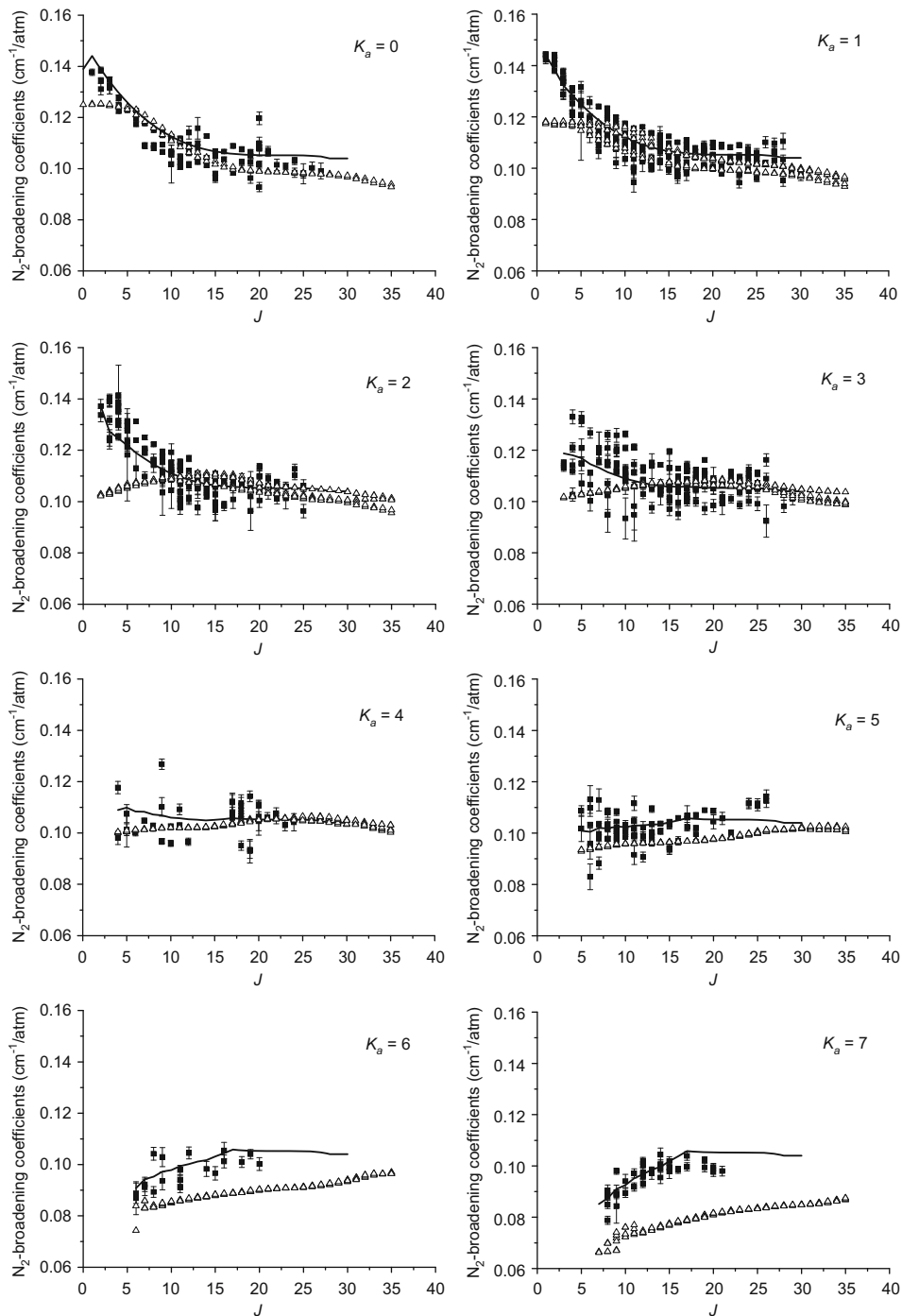
**Fig. 8.** $N_2$-broadening coefficients measurements are plotted (solid squares) for each value of $K_a$ (from 0 up to 7). The error bars are 1SD. The continuous line represents calculation based on an empirical expansion (see Eq. (1)) and parameters of Table 2. Open triangles are the theoretical calculation using the Complex Robert–Bonamy Formalism for $\Delta K_a = 0$ transitions (see Section 4).

was taken and 3296 $\nu_2$ transitions extracted for this study. Complex Robert–Bonamy calculations of the half-width were made at 7 temperatures (200, 225, 275, 296, 350, 500, and 700 K) by solving Eq. (2). The calculations are for transitions with $J=0-41$ and $K_a=0-16$. The half-widths at 296 K range from roughly 0.02–0.128, a factor of 6.4.

The power law model for the temperature dependence of the half-width was given by Birnbaum [41] by considering a one term intermolecular potential and all on-resonance collisions giving

$$\gamma(T) = \gamma(T_0)\left[\frac{T_0}{T}\right]^n \tag{3}$$

**Table 3**
Initial and final atom–atom parameters for the $H_2CO$–$N_2$ collision systems.

| Interacting pair | $\varepsilon_{initial}/k_B$ (K) | $\varepsilon_{final}/k_B$ (K) | $\varepsilon_{initial}$ (Å) | $\varepsilon_{final}$ (Å) |
|---|---|---|---|---|
| H–N | 20.45 | 13.2925 | 2.99 | 1.9435 |
| C–N | 33.75 | 21.9375 | 3.42 | 2.223 |
| O–N | 43.88 | 28.5220 | 3.148 | 2.0462 |

**Table 4**
Measured and calculated $N_2$-broadening coefficients (in $cm^{-1}\,atm^{-1}$) noted *Exp* and *Calc*, respectively, for the 39 chosen lines.

| Rot′ | | | Rot″ | | | Exp | Calc | Dif |
|---|---|---|---|---|---|---|---|---|
| 23 | 1 | 23 | 24 | 1 | 24 | 0.10360 | 0.10025 | 3.2 |
| 21 | 3 | 18 | 22 | 3 | 19 | 0.11000 | 0.10917 | 0.8 |
| 21 | 3 | 19 | 22 | 3 | 20 | 0.11150 | 0.10702 | 4.0 |
| 17 | 0 | 17 | 18 | 0 | 18 | 0.10760 | 0.10106 | 6.1 |
| 16 | 2 | 15 | 17 | 2 | 16 | 0.10750 | 0.10667 | 0.8 |
| 15 | 2 | 13 | 16 | 2 | 14 | 0.10620 | 0.11147 | −5.0 |
| 18 | 2 | 17 | 17 | 2 | 16 | 0.10670 | 0.10595 | 0.7 |
| 18 | 2 | 16 | 17 | 2 | 15 | 0.10550 | 0.11069 | −4.9 |
| 19 | 2 | 18 | 18 | 2 | 17 | 0.10660 | 0.10530 | 1.2 |
| 20 | 0 | 20 | 19 | 0 | 19 | 0.10660 | 0.10032 | 5.9 |
| 23 | 3 | 21 | 22 | 3 | 20 | 0.10800 | 0.10665 | 1.3 |
| 25 | 1 | 25 | 24 | 1 | 24 | 0.10460 | 0.09976 | 4.6 |
| 23 | 3 | 20 | 22 | 3 | 19 | 0.10840 | 0.10880 | −0.4 |
| 24 | 1 | 23 | 23 | 1 | 22 | 0.10460 | 0.10324 | 1.3 |
| 12 | 0 | 12 | 12 | 1 | 11 | 0.10740 | 0.11244 | −4.7 |
| 22 | 1 | 22 | 23 | 1 | 23 | 0.09760 | 0.10039 | −2.9 |
| 19 | 3 | 17 | 20 | 3 | 18 | 0.10830 | 0.10741 | 0.8 |
| 16 | 0 | 16 | 17 | 0 | 17 | 0.09840 | 0.10188 | −3.5 |
| 14 | 2 | 13 | 15 | 2 | 14 | 0.10280 | 0.10768 | −4.7 |
| 12 | 2 | 10 | 12 | 1 | 11 | 0.10330 | 0.11304 | −9.4 |
| 14 | 0 | 14 | 13 | 1 | 13 | 0.10850 | 0.10485 | 3.4 |
| 15 | 2 | 13 | 16 | 3 | 14 | 0.10940 | 0.11162 | −2.0 |
| 2 | 0 | 2 | 3 | 0 | 3 | 0.13470 | 0.12574 | 6.7 |
| 15 | 1 | 15 | 16 | 0 | 16 | 0.10360 | 0.10279 | 0.8 |
| 19 | 0 | 19 | 19 | 1 | 18 | 0.10660 | 0.10436 | 2.1 |
| 16 | 1 | 15 | 16 | 2 | 14 | 0.09860 | 0.11080 | −12.4 |
| 22 | 3 | 20 | 21 | 3 | 19 | 0.10080 | 0.10705 | −6.2 |
| 23 | 3 | 21 | 22 | 3 | 20 | 0.10100 | 0.10665 | −5.6 |
| 24 | 1 | 24 | 23 | 1 | 23 | 0.10440 | 0.10017 | 4.1 |
| 3 | 1 | 3 | 2 | 0 | 2 | 0.13110 | 0.12331 | 5.9 |
| 22 | 2 | 20 | 22 | 1 | 21 | 0.10240 | 0.10655 | −4.1 |
| 9 | 3 | 6 | 9 | 2 | 7 | 0.10810 | 0.10889 | −0.7 |
| 18 | 4 | 15 | 18 | 3 | 16 | 0.10530 | 0.10767 | −2.3 |
| 25 | 0 | 25 | 24 | 1 | 24 | 0.10750 | 0.09970 | 7.3 |
| 20 | 2 | 19 | 19 | 1 | 18 | 0.10040 | 0.10669 | −6.3 |
| 21 | 2 | 20 | 20 | 1 | 19 | 0.10350 | 0.10617 | −2.6 |
| 13 | 2 | 11 | 12 | 1 | 12 | 0.10530 | 0.11008 | −4.5 |
| 17 | 4 | 14 | 16 | 3 | 13 | 0.10540 | 0.10791 | −2.4 |
| 17 | 4 | 13 | 16 | 3 | 14 | 0.09930 | 0.10775 | −8.5 |

Rotational quantum numbers ($J$, $K_a$, $K_c$) are given for both the upper state (*Rot′*), and the lower one (*Rot″*). *Dif* is the *Exp–Calc* difference in %.

where $n$ is called the temperature exponent. While modern calculations use hundreds of terms in the intermolecular potential, Eq. (3) remains a reliable model for many systems. However, the correctness of Eq. (3) does need to be tested as discussed below.

The temperature exponent does depend on the temperature range of the fit [42,43]. Here, the temperature exponent was determined for each transition by a least-squares fit of $ln[\gamma(T)/\gamma(T_0)]$ vs $ln[T_0/T]$ using five (200–350 K) and seven (200–700 K) temperatures of the study. The error in the temperature exponent was

determined as follows: The temperature exponents were calculated using the half-width values at any two of the temperatures studied. For example, with seven temperatures this yields twenty-one 2-point temperature exponents. The difference between each 2-point temperature exponent and the least-squares fit value is calculated. The error is taken as the largest of these differences. While this procedure tends to yield the maximum error in the temperature exponent, given the nature of the data and other uncertainties it is thought to be more reasonable than a statistical value taken from the fit.

The half-widths at 296 K are plotted versus an energy ordered index ($J(J+1)+K_a-K_c+1$) in Fig. 9 where the plot symbols are the $K_a$ values. The roughly vertical columns in the figure are data with the same $J$. There appears to be some structure with respect to the $K_a$ with the largest half-widths belonging to transitions with the smallest $K_a$ values. However, no simple propensity rule to accurately predict half-widths can be derived from the data.

## 5. Comparisons

Fig. 10 shows the measured half-widths from Refs. [48–51] and this work and the calculated half-widths versus $J+0.9(K_a/J)$. The star symbols are the measurements of the $\nu_3$ band transitions by Cline and Varghese [48], The square symbol is the measurement of Burkart and Schramm on the $4_{1\ 4}\leftarrow5_{1\ 5}$ transition in the $\nu_1$ band [49], the open circle with the plus sign symbol is the measurement of the $3_{1\ 3}\leftarrow3_{1\ 2}$ transition in the rotation band [50], the open plus sign symbol is the measurement of the the $3_{0\ 3}\leftarrow3_{1\ 3}$ transition in the $\nu_4$ band by Nadler et al. [51], the solid triangles are the measurements of this work (plotted only for transitions with $K_a$=0–3). All the measurements have the associated error bars plotted as well. The solid circles are the CRB calculations of the half-widths for $\nu_2$ transitions (plotted only for transitions with $K_a$=0, 1, 2 and 3). The plot shows the data of refs. [49] and [51] are low compared with the other measurements. It is not certain if this is an effect of vibrational dependence of the half-widths for these two transitions. The data of Ref. [48] agree somewhat with the measurements made here at low $J$ but the data above $J$=8 have smaller values than the measurements made here. The calculated half-widths are lower than the measurements made here for low $J$. For $J \geq 5$ the agreement is good. Overall the calculations have a 3.3% difference when compared with 354 measurements.

## 6. Temperature dependence of the half-width

The temperature dependence of the $N_2$-broadened widths is necessary to describe accurately the atmospheric spectra of $H_2CO$. No measurements have been performed in this work or in literature, so that the theoretical calculation presented in this paper has been used to derive the temperature dependence coefficients.

The temperature dependence of the $N_2$-broadened half-widths was determined for the 3296 $\nu_2$ band transitions studied in this work using the power law
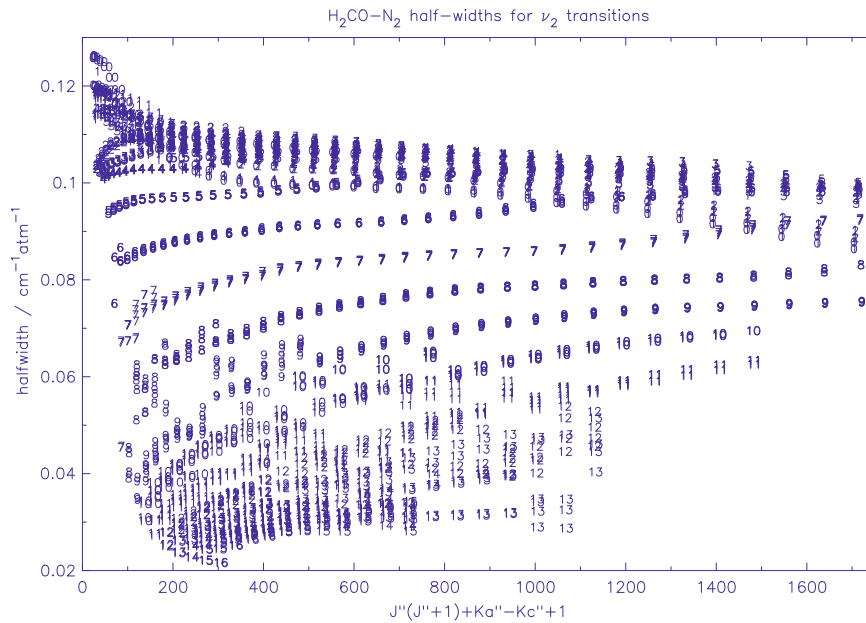
**Fig. 9.** $H_2CO$ $N_2$-broadened half-widths at 296 K plotted versus an energy ordered index $(J(J+1)+K_a-K_c+1)$ where the plot symbols are the $K_a$ values.
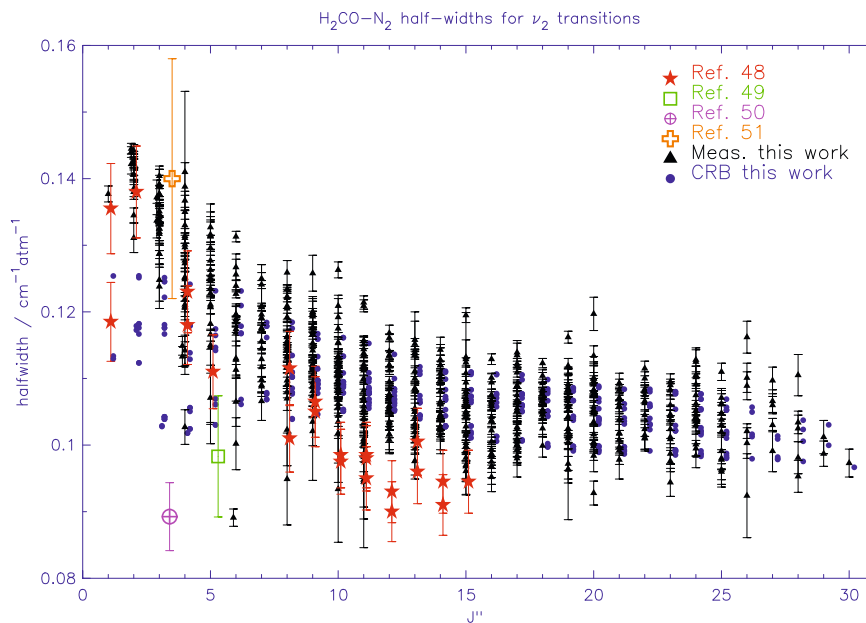


**Fig. 10.** Comparison between the measured and calculated $N_2$-broadened half-widths of $H_2CO$ at 296 K, and measurements from literature. Note that data are shifted as a function of reference so that they do not overlap.

formula, Eq. (3). The "rule-of-thumb" expression for the temperature exponent given by Birnbaum [41] for a "dipole–quadrupole" system, such as $H_2CO$–$N_2$ states that $n=5/6$.

Some recent studies have shown that for certain types of radiator–perturber interactions the power law model is questionable. Wagner et al. [44] have observed that for certain transitions of water vapor perturbed by air, $N_2$ or $O_2$ the power law does not correctly model the temperature dependence of the half-width. This fact was later demonstrated by Toth et al. [45] in a study of air-broadening of water vapor transitions in the region from 696–2163 $cm^{-1}$. In both studies it was found that the temperature exponent, $n$, can be negative for many transitions. In such cases the power law model, Eq. (3), is not completely correct. The mechanism leading to negative temperature exponents is called the resonance overtaking effect and was discussed by Hartmann et al. [46], Wagner et al. [44], and Antony et al. [47]. Thus, in this work the applicability of the power law model was tested.
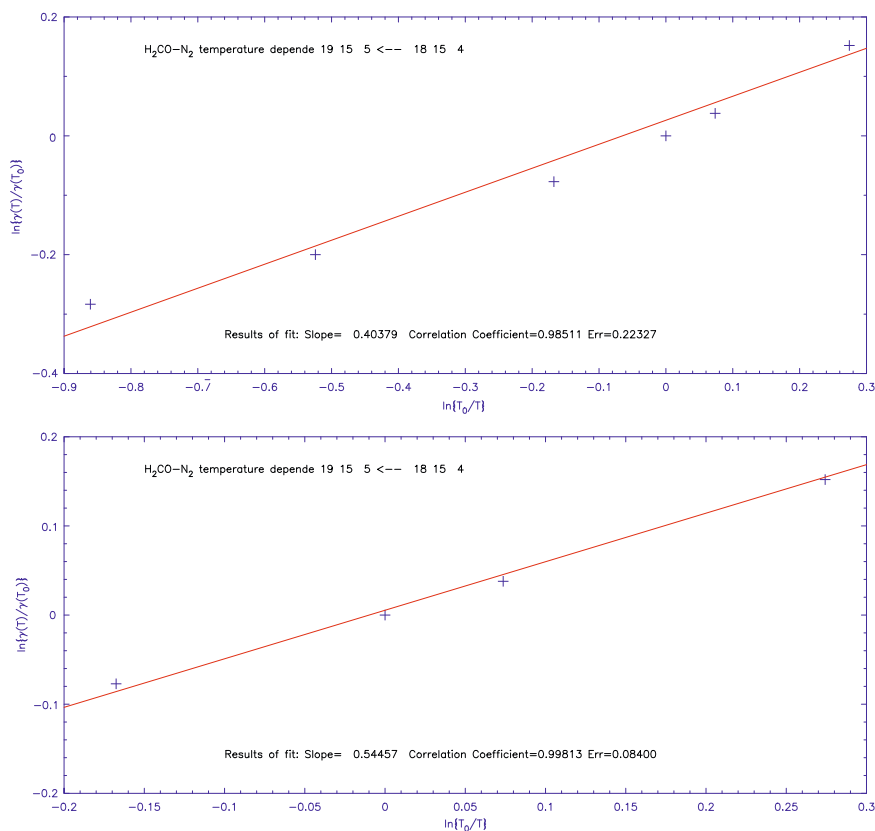
**Fig. 11.** Temperature exponent of the $19_{15\ 5} \leftarrow 18_{15\ 4}$ transition obtained for the two temperature ranges.

The values for the temperature dependence of the $N_2$-broadened half-width go from roughly 0.83–0.10. While the range in values is large, there are no negative temperature exponents for this collision system. As stated above the temperature exponents were calculated for 2 temperature ranges; 200–350 K, and 200–700 K. Fig. 11 shows the fits for the $19_{15\ 5} \leftarrow 18_{15\ 4}$ transition for the two temperature ranges. Plotted are $ln[\gamma(T)/\gamma(T_0)]$ versus $ln[T_0/T]$ where the slope of the fitted line is the value of $n$. The temperature exponent for the 7 data points is 0.40 (top panel) and that for the 5-point fit is 0.54 (bottom panel). For both cases the correlation coefficient, $R$, indicates the power law fit is not perfect and the error associated with the 7-point fit is almost 3 times larger than that for the 5-point fit. (Note, the scale of the abscissa is different in each panel.) For atmospheric applications the temperature range of the 5-point fit, 200–350 K, is more appropriate and the temperature exponents reported here are those of the 5-point fit. In Fig. 12 $ln[\gamma(T)/\gamma(T_0)]$ versus $ln[T_0/T]$ is plotted for the $2_{1\ 1} \leftarrow 2_{1\ 2}$ transition (top panel) and the $20_{14\ 6} \leftarrow 19_{14\ 5}$ transition (lower panel). In the top panel the fit is quite good ($R=0.99995$) and the slope, $n$, is 0.761(0.038). In the lower panels is an example of a high $J$ and $K_a$ transition where $n$ is 0.360(0.240) the fit is not as good ($R=0.9831$), which is reflected in the reported error. It is cautioned that there are many transitions, especially high $J$ and $K_a$ transitions, for which the power law model does not work well.

In Fig. 13 the temperature exponents for the 3296 $N_2$-broadened transitions of $H_2CO$ are plotted versus energy ordered index. The dashed line in the plot is the "rule of thumb" value, 5/6. Plots (not shown here) were made with $K_a$ as the plot symbol and different coordinates for the abscissa but no structure was evident. Fig. 13 shows there are large variations in $n$ as a function of the rotational quantum numbers.

## 7. Creation of a complete line list

The last edition of HITRAN [13] contain the recent line list of Perrin et al. [12] concerning both the 3.6 and 5.7 μm spectral regions (35 958 lines), and data for the 0–100 cm$^{-1}$ spectral region (163 lines). For all these transitions, constant values have been used for both the self- and $N_2$-broadening coefficients, as well as for the temperature dependence of the $N_2$-broadening coefficients. The aim was here to generate self- and air-broadening coefficients, but also temperature dependence of the air-broadened widths for all the transitions of HITRAN 2008 [13]. In HITRAN 2008, for the 611 pure rotational transitions (up to 100 cm$^{-1}$) the self- and air-broadening coefficients have a default value of 0.000 and 0.107 cm$^{-1}$, respectively, and the temperature exponent for the air-width is equal to 0.5. In the 3.6 and 5.7 μm spectral region 11 and 3 bands are present in HITRAN 2008 (see Tables 1 and 9 of Ref. [12]): the self- and
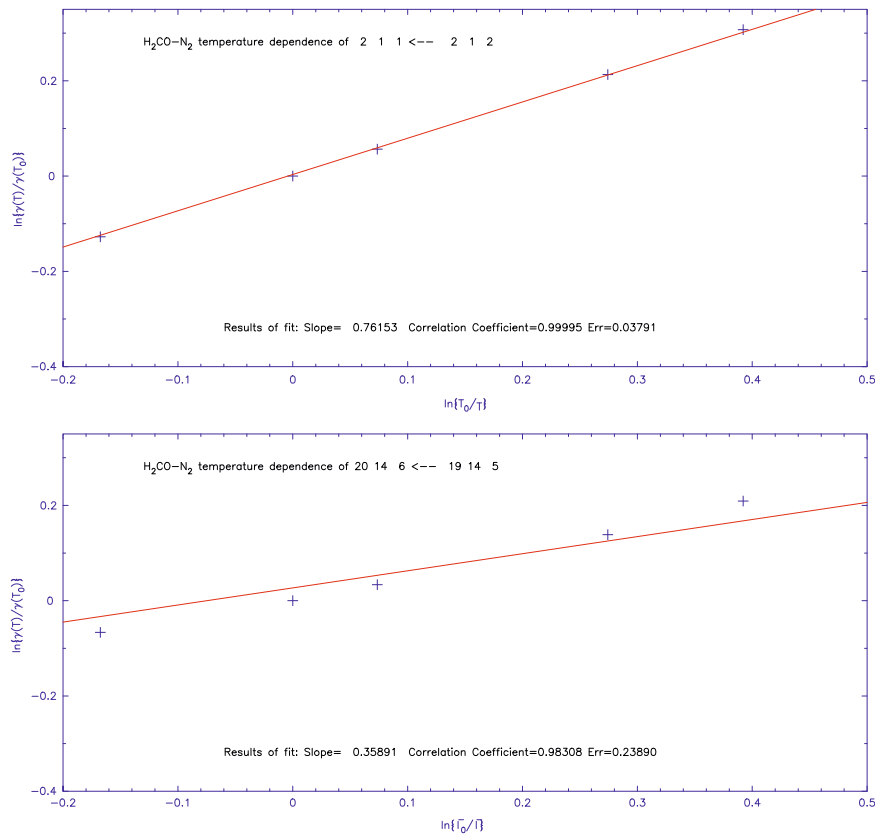
**Fig. 12.** Temperature exponents of the $2_{1\ 1} \leftarrow 2_{1\ 2}$ and the $20_{14\ 6} \leftarrow 19_{14\ 5}$ transitions obtained for the 200–350 K range with the 5-point fit.
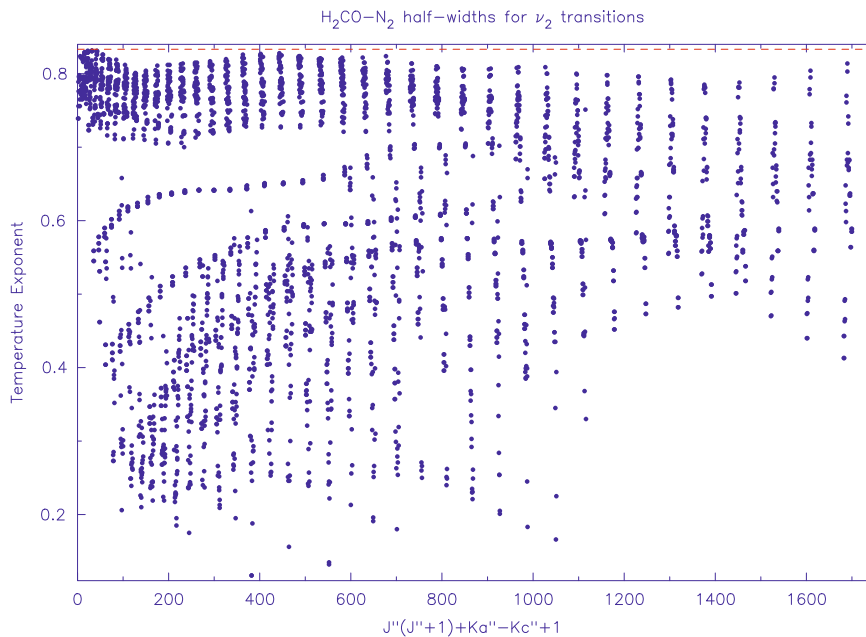


**Fig. 13.** Temperature exponents for the 3296 $N_2$-broadened transitions of $H_2CO$ plotted versus the energy ordered index.

air-broadening coefficients have a default value of 0.000 and 0.108 cm$^{-1}$, respectively, and the temperature exponent for the air-width is equal to 0.7.

The supplementary line list given in Table A3, is based on HITRAN 2008 transitions. For each transitions, based only on the rotational quantum numbers of the lower

state, self- and $N_2$-broadened half-widths have been generated using the empirical polynomial expansion (Eq. (1)) and the parameters of Table 2 (see Section 3.2), neglecting any vibrational dependence. In a same way, the complex Robert–Bonamy calculations for the $v_2$ band (see Section 3.3) have also been used to generate scaled air-broadening coefficients and their temperature dependence. When possible the CRB calculations are used for other vibrational bands (neglect of vibrational dependence) by matching the lower and upper state rotational quantum numbers of the transitions. The air-broadening have been approximated by multiplying the $N_2$-broadened half-widths by 0.94, and the temperature exponents for air have been supposed to be identical as the one for $N_2$.

## Acknowledgments

## Appendix A.  Supplementary material

Supplementary data associated with this article can be found in the online version at doi:10.1016/j.jqsrt.2010.02.004.

## References

[1] Yokelson RJ, Goode JG, Ward DE, Susott RA, Babbitt RE, Wade DD, et al. Emissions of formaldehyde, acetic acid, methanol, and other trace gases from biomass fires in North Carolina measured by airborne Fourier transform infrared spectroscopy. J Geophys Res 1999;D104:30109–25.

[2] Fried A, Sewell S, Henry B, Wert BP, Gilpin T. Tunable diode laser absorption spectrometer for ground-based measurements of formaldehyde. J Geophys Res 1997;D102:6253–66.

[3] Fried A, Lee YN, Frost G, Wert B, Henry B, Drummond JR, et al. Airborne $CH_2O$ measurements over the North Atlantic during the 1997 NARE campaign: instrument comparisons and distributions. J Geophys Res 2002;D107 ACH14-1–21.

[4] Wert BP, Fried A, Rauenbuehler S, Walega J, Henry B. Design and performance of a tunable diode laser absorption spectrometer for airborne formaldehyde measurements. J Geophys Res 2003; 108(D12) ACH1-1–15.

[5] Richter D, Fried A, Wert BP, Walega JG, Tittel FK. Development of a tunable mid-IR difference frequency laser source for highly sensitive airborne trace gas detection. Appl Phys 2002;B75:281–8.

[6] Dahnke H, von Basum G, Kleinermanns K, Hering P, Murts M. Rapid formaldehyde monitoring in ambient air by means of mid-infrared cavity leak-out spectroscopy. Appl Phys 2002;B75:311–6.

[7] Coheur PF, Herbin H, Clerbaux C, Hurtmans D, Wespes C, Carleer M, et al. ACE-FTS observation of a young biomass burning plume: first reported measurements of $C_2H_4$, $C_3H_6O$, $H_2CO$ and PAN by infrared occultation from space. Atmos Chem Phys 2007;7:5437–46.

[8] Wagner V, Schiller C, Fischer H. Formaldehyde measurements in the marine boundary layer of the Indian Ocean during the 1999 INDOEX cruise of the R/V Ronald H. Brown. J Geophys Res 2001;D106:28528–38.

[9] Steck T, Glatthor N, von Clarmann T, Fischer H, Flaud JM, Funke B, et al. Retrieval of global upper tropospheric and stratospheric formaldehyde (H2CO) distributions from high-resolution MIPAS-Envisat spectra. Atmos Chem Phys 2008;8:463–70.

[10] Herndon SC, Zahniser MS, Nelson Jr DD, Shorter J, McManus JB, Jimenez R, et al. Airborne measurements of HCHO and HCOOH during the New England air quality study 2004 using a pulsed quantum cascade laser spectrometer. J Geophys Res 2007;112(D10) D10S03-1–15.

[11] Rinsland CP, Goldman A. Infrared spectroscopic measurements of tropospheric trace gases. Appl Opt 1992;31:6969–71.

[12] Perrin A, Jacquemart D, Kwabia Tchana F, Lacome N. Absolute line intensities and new linelists for the 5.7 and 3.6 μm bands of formaldehyde. JQSRT 2009;110:700–16.

[13] Rothman LS, Gordon IE, Barbe A, Chris Benner D, Bernath PF, Birk M, et al. The HITRAN 2008 molecular spectroscopic database. JQSRT 2009;110:533–72.

[14] Jacquemart D, Mandin JY, Dana V, Picqué N, Guelachvili G. A multispectrum fitting procedure to deduce molecular line parameters. Application to the 3–0 band of $^{12}C^{16}O$. Eur Phys J D 2001;14:55–69.

[15] Nemtchinov V, Sung K, Varanasi P. Measurements of line intensities and half-widths in the 10-μm bands of $^{14}NH_3$. JQSRT 2004;83: 243–65.

[16] Predoi-Cross A, Hambrook K, Brawley-Tremblay S, Bouanich JP, Malathy Devi V, Smith MAH. Room-temperature broadening and pressure-shift coefficients in the $v_2$ band of $CH_3D$–$O_2$: measurements and semi-classical calculations. J Mol Spectrosc 2006;236: 75–90.

[17] Predoi-Cross A, Hambrook K, Brawley-Tremblay S, Bouanich JP, Malathy Devi V, Smith MAH. Measurements and theoretical calculations of $N_2$-broadening and $N_2$-shifting coefficients in the $v_2$ band of $CH_3D$. J Mol Spectrosc 2006;235:35–53.

[18] Lepère M, Blanquet G, Walrand J, Bouanich JP. $K$-dependence of broadening coefficients for $CH_3F$–$N_2$ and for other systems involving a symmetric top molecule. J Mol Spectrosc 2000; 517–518:493–502.

[19] Chackerian C, Brown LR, Lacome N, Tarrago G. Methyl chloride $v_5$ region lineshape parameters and rotational constants for the $v_2$, $v_5$, and $2v_3$ vibrational bands. J Mol Spectrosc 1998;191: 148–57.

[20] Bouanich JP, Blanquet G, Walrand J. Theoretical $O_2$-and $N_2$-broadening coefficients of $CH_3Cl$ spectral lines. J Mol Spectrosc 1993;161:416–26.

[21] Levy A, Lacome N, Tarrago G. Hydrogen-and helium-broadening phosphine lines. J Mol Spectrosc 1993;157:172–81.

[22] Jacquemart D, Kwabia Tchana F, Lacome N, Kleiner I. A complete set of line parameters for $CH_3Br$ in the 10-μm spectral region. JQSRT 2007;105:264–302.

[23] Lynch R. Half-widths and line shifts of water vapor perturbed by both nitrogen and oxygen. PhD dissertation, University of Massachusetts Lowell; June 1995.

[24] Lynch R, Gamache RR, Neshyba SP. Fully complex implementation of the Robert-Bonamy formalism: halfwidths and line shifts of $H_2O$ broadened by $N_2$. J Chem Phys 1996;105:5711–21.

[25] Gamache RR, Lynch R, Neshyba SP. New developments in the theory of pressure-broadening and pressure-shifting of spectral lines of $H_2O$: the complex Robert-Bonamy formalism. JQSRT 1998;59:319–35.

[26] Robert D, Bonamy J. Short range force effects in semiclassical molecular line broadening calculations. J De Phys 1979;20: 923–43.

[27] Baranger M. General impact theory of pressure broadening. Phys Rev 1958;112:855–65.

[28] Ben-Reuven A. Spectral line shapes in gases in the binary-collision approximation. In: Prigogine I, Rice SA, editors. Advances in chemical physics. New York: Academic Press; 1975. p. 235.

[29] Hirschfelder JO, Curtiss CF, Bird RB. Molecular theory of gases and liquids. New York: Wiley; 1964.

[30] Sack RA. Two-center expansion for the powers of the distance between two points. J Math Phys 1964;5:260–8.

[31] Neshyba SP, Gamache RR. Improved line broadening coefficients for asymmetric rotor molecules: application to ozone perturbed by nitrogen. JQSRT 1993;50:443–53.

[32] Neshyba SP, Lynch R, Gamache RR, Gabard T, Champion JP. Pressure induced widths and shifts for the $v_3$ band of methane. J Chem Phys 1994;101:9412–21.

[33] Watson JKG. Determination of centrifugal distortion coefficients of asymmetric-top molecules. J Chem Phys 1967;46:1935–49.

[34] Muller HSP, Winnewisser G, Demasion J, Perrin A, Valentin A. The ground state spectroscopic constants of formaldehyde. J Mol Spectrosc 2000;200:143–4.

[35] Perrin A. Watson Hamiltonian constants for the $\nu_2$ band of $H_2CO$ and $H_2CO$ linelist. Private communication, Laboratoire Inter-Universitaire des Systemes Atmospheriques (LISA), CNRS, Universite Paris XII, Paris, France; 2007.

[36] Huber KP, Herzberg G. Molecular spectra and molecular structure: constants of diatomic molecules. New York: Van Nostrand; 1979.

[37] Fabricant B, Krieger D, Muebnter JS. Molecular beam electric resonance study of formaldehyde, thioformaldehyde, and ketene. J Chem Phys 1977;67:1576–86.

[38] Kukolich SG. Molecular beam measurements of the magnetic susceptibility anisotrophies and molecular quadrupole moment in $H_2CO$. J Chem Phys 1971;54:8–11.

[39] Mulder F, van Dijk G, van der Avoird A. Multipole moments, polarizabilities and anisotropic long range interaction coefficients for $N_2$. Mol Phys 1980;39:407–25.

[40] Bouanich J-P. Site-site Lennard–Jones potential parameters for $N_2$ , $O_2$ , $H_2$, CO and $CO_2$. JQSRT 1992;47:243–50.

[41] Birnbaum G. Microwave pressure broadening and its application to intermolecular forces. Adv Chem Phys 1967;12:487–548.

[42] Brown LR, Humphrey CM, Gamache RR. $CO_2$-broadened water in the pure rotation and $\nu_2$ fundamental regions. J Mol Spectrosc 2007;246:1–21.

[43] Gamache RR, Laraia AA. $N_2$-, $O_2$-, and air-broadened half-widths, their temperature dependence, and line shifts for the rotation band of $H_2^{16}O$. J Mol Spectrosc 2009;257:116–27.

[44] Wagner G, Birk M, Gamache RR, Hartmann JM. Collisional parameters of $H_2O$ lines: effects of temperature. JQSRT 2005;92:211–30.

[45] Toth RA, Brown LR, Smith MAH, Malathy Devi V, Chris Benner D, Dulick M. Air-broadening of $H_2O$ as a function of temperature: 696–2163 $cm^{-1}$. JQSRT 2006;101:339–66.

[46] Hartmann JM, Taine J, Bonamy J, Labani B, Robert D. Collisional broadening of rotation-vibration lines for asymmetric-top molecules II. $H_2O$ diode laser measurements in the 400–900 K range; calculations in the 300–2000 K range. J Chem Phys 1987;86:144–56.

[47] Antony BK, Neshyba S, Gamache RR. Self-broadening of water vapor transitions via the complex Robert–Bonamy theory. JQSRT 2006;105:148–63.

[48] Cline DS, Varghese PL. High resolution spectral measurements in the $\nu_5$ band of formaldehyde using a tunable IR diode laser. Appl Opt 1988;27:3219–24.

[49] Burkart M, Schramm B. Foreign gasbroadening of an IR absorption line of formaldehyde. J Mol Spectrosc 2003;217:153–6.

[50] Srivastava GP, Gautam HO, Kumar A. Microwave pressure broadening studies of some molecules. J Phys B Atom Mol Phys 1973;6:743–55.

[51] Nadler S, Daunt SJ, Reuter DC. Tunable diode laser measurements of formaldehyde foreign gas broadening parameters and line strengths in the 9–11 μm region. Appl Opt 1987;26:1641–6.